Paper AAS 04-129

Angle-of-Attack-Modulated Terminal Point Control for Neptune Aerocapture

Eric M. Queen

NASA Langley Research Center
Hampton Va 23681-2199

14th AAS/AIAA Space Flight Mechanics Conference

Maui, Hawaii, February 8-12, 2004

AAS Publications Office, P.O. Box 28130, San Diego, CA 92198

ANGLE-OF-ATTACK-MODULATED TERMINAL POINT CONTROL FOR NEPTUNE AEROCAPTURE

Eric M. Queen†

An aerocapture guidance algorithm based on a calculus of variations approach is developed, using angle of attack as the primary control variable. Bank angle is used as a secondary control to alleviate angle of attack extremes and to control inclination. The guidance equations are derived in detail. The controller has very small onboard computational requirements and is robust to atmospheric and aerodynamic dispersions. The algorithm is applied to aerocapture at Neptune. Three versions of the controller are considered with varying angle of attack authority. The three versions of the controller are evaluated using Monte Carlo simulations with expected dispersions.

INTRODUCTION

"Aerocapture" is the use of aerodynamic forces to capture a satellite into an elliptic orbit from a hyperbolic approach orbit. Because aerocapture promises great reductions in mass needed to achieve orbit about certain planets, it has been proposed for several advanced missions. [1, 2, 3] Often, the vehicles used for these missions are blunt bodies with a small, nearly constant lift-to-drag ratio (L/D). This approach has heritage dating back to the Apollo era. [4] The blunt body configurations considered have been designed to fly at a constant angle of attack. The trajectories flown by these vehicles have been controlled by modulation of the bank angle. Bank angle magnitude is used to control the apoapsis altitude and sign of the bank angle is used to control the inclination or wedge angle.

Recently, a mission has been proposed for aerocapture at Neptune. Neptune's deep gravity well leads to very high entry velocities, on the order of 30 km/s. For these high entry velocities, bank angle modulation may not provide sufficient control authority to ensure accurate aerocapture. To overcome this issue, a combination of angle of attack modulation and bank angle modulation may be required.

The guidance algorithm for the Apollo Earth return used a terminal point controller based on calculus-of-variations theory for the final phase of flight [5]. Later, this approach was applied to aerocapture using bank angle modulation as the control [6, 7]. The current work develops a terminal point controller for aerocapture with angle of attack as the control variable. This type of controller is desirable for several reasons. The first is small computational requirements. The current engineering code is about 350 lines for the onboard portion of the algorithm, with no iterative loops. Also, for the types of dispersions and uncertainties expected, experience has shown the algorithm to be relatively robust. Perhaps most importantly, when the algorithm is pushed beyond reasonable limits, it degrades gracefully.

The General Theory section gives details of the mathematical formulation of a two-point boundary value problem. The section on Application to Aerocapture applies this process to the problem of aerocapture. The Mission section gives a brief description of the Neptune Aerocapture mission. The Numerical Results section shows results of numerical Monte Carlo simulations that were performed to establish performance of the algorithm.

†NASA Langley Research Center, Hampton, Va

GENERAL THEORY

The general theory of terminal point control is widely available. See, for instance, Applied Optimal Control by Bryson and Ho[5]. The following development follows Bryson and Ho.

Consider a system described by differential equations

$$\dot{x} = f(x, u, t) \tag{1}$$

with x(t0) given. For aerocapture, it is convenient to write the cost function as:

$$J = \phi(x(t_f), t_f) \tag{2}$$

after adjoining the differential equations 1 to equation 2 and integrating by parts:

$$J = \phi(x(t_f), t_f) - \lambda^T(t_f)x(t_f) + \lambda^T(t_0)x(t_0) + \int_{t_0}^{t_f} \left[\lambda^T(t)f(x, u, t) + \dot{\lambda}^T(t)x(t)\right] dt \tag{3}$$

Next consider the first order variations in J

$$\delta J = \left[\left(\frac{\partial \phi}{\partial x} - \lambda^T\right)\delta x\right]_{t=t_f} + \left[\lambda^T \delta x\right]_{t=t_0} + \int_{t_0}^{t_f} \left[\left(\lambda^T \frac{\partial f}{\partial x} + \dot{\lambda}^T\right)\delta x + \left(\lambda^T \frac{\partial f}{\partial u}\right)\delta u\right] dt \tag{4}$$

A convenient choice for λ is:

$$\dot{\lambda} = -\lambda^T \frac{\partial f}{\partial x} \tag{5}$$

with boundary conditions

$$\lambda^T(t_f) = \frac{\partial \phi(t_f)}{\partial x(t_f)} \tag{6}$$

which yields

$$\delta J = \left[\lambda^T \delta x\right]_{t=t_0} + \int_{t_0}^{t_f} \left[\left(\lambda^T \frac{\partial f}{\partial u}\right)\delta u\right] dt \tag{7}$$

Particular solutions to the differential equations are:[6]

$$\delta x(t) = \frac{1}{\lambda(t)}\left[\lambda^T(t_0)\delta x(t_0) + \int_{t_0}^{t_f} \left[\left(\lambda^T \frac{\partial f}{\partial u}\right)\delta u\right] dt\right] \tag{8}$$

and

$$\lambda(t) = e^{\int \frac{\partial f}{\partial x} dt} \tag{9}$$

From equations 7 and 8 it follows that

$$\delta J = \lambda^T(t)\delta x(t) \tag{10}$$

Which means that we have linearized the change in cost function with respect to deviations in the states. The coefficients in the linear equations are determined by equations 5 and 6.

APPLICATION TO AEROCAPTURE

In-Plane control

The relevant performance index J for aerocapture is ΔV, the change in velocity required to reach the desired orbit. A nominal trajectory will be determined which has a value of ΔV that is acceptable to the mission (preferably small) a guidance which drives δJ to zero will maintain ΔV near the nominal value.

We take as our state

$$\mathbf{x}(t) = \begin{bmatrix} V(t) \\ \gamma(t) \\ h(t) \end{bmatrix} \tag{11}$$

with state equation

$$\mathbf{f}(\mathbf{x}(t), \mathbf{u}(t)) = \begin{bmatrix} -\left(\frac{D}{m} + g\sin(\gamma)\right) \\ \frac{L\cos(\phi)}{mV} + \left(\frac{V}{r_e+h} - \frac{g}{V}\right)\cos(\gamma) \\ V\sin(\gamma) \end{bmatrix} \tag{12}$$

and costates

$$\lambda(t) = \begin{bmatrix} \lambda_V(t) \\ \lambda_\gamma(t) \\ \lambda_h(t) \end{bmatrix} \tag{13}$$

which leads to:

$$\frac{\partial \mathbf{f}}{\partial \mathbf{x}^*} = \begin{bmatrix} \frac{-2D^*}{V^* m} & g\cos(\gamma^*) & \frac{D^*/m}{h_s} \\ \frac{L^*\cos(\phi)}{m(V^*)^2} + \left(\frac{1}{r_e+h} - \frac{g}{(V^*)2}\right)\cos(\gamma) & \left(\frac{g}{V^*} - \frac{V^*}{r_e+h^*}\right)\sin(\gamma^*) & \frac{L^*\cos(\phi)}{mV^* h_s^*} + \frac{V^*\cos(\gamma^*)}{(r_e+h^*)^2} \\ \sin(\gamma^*) & V^*\cos(\gamma^*) & 0 \end{bmatrix} \tag{14}$$

where the superscript $*$ indicates values taken from a nominal trajectory. Taking ΔV as our performance index, equation 7 becomes

$$\delta\Delta V = \left[\lambda^T \delta x\right]_{t=t_0} + \int_{t_0}^{t_f} \left[\left(\lambda^T \frac{\partial f}{\partial u}\right)\delta u\right] dt \tag{15}$$

with

$$\lambda^T(t_f) = \frac{\partial \Delta V(t_f)}{\partial x(t_f)} \tag{16}$$

Which is a two-point boundary value problem. To solve this problem, we set $\delta\Delta V = 0$ and solve for the control δu. Unfortunately, the solution for δu is impossible unless we assume a form for δu. For convenience, we will assume δu is a constant and a scalar. In which case we have

$$\delta u = \frac{-\lambda^T \delta x\big|_{t=t_0}}{\int_{t_0}^{t_f} \left(\frac{\partial f^T}{\partial u}\lambda\right) dt} \tag{17}$$

we define

$$\lambda_u(t) = \int_t^{t_f} \lambda^T \left(\frac{\partial f^T}{\partial u}\right) dt \tag{18}$$

After some manipulation the time derivative of λu is determined to be:

$$\frac{d\lambda_u}{dt} = -\lambda^T(t)\frac{\partial f(t)}{\partial u(t)} \tag{19}$$

and

$$\lambda_u(t_f) = 0 \tag{20}$$

Equation 17 expands to

$$\delta u = \frac{\lambda_h \delta h + \lambda_V \delta V + \lambda_\gamma \delta\gamma}{\lambda_u} \tag{21}$$

Taking the first partial of $\dot{h}$ with respect to γ yields

$$\delta\gamma = \frac{\delta\dot{h}}{V\cos(\gamma)} \tag{22}$$

We assume

$$D = \frac{1}{2}\rho_0 \exp(-h/h_s)V^2 C_d A \tag{23}$$

and take the partial of D/m with respect to h yields

$$\delta h = -\frac{\delta\,(D/m)\,m h_s}{D} \tag{24}$$

Substituting into equation 21 we have

$$\delta u = \frac{-\lambda_h \frac{\delta(D/m)mh_s}{D} + \lambda_V \delta V + \lambda_\gamma \frac{\delta\dot{h}}{V\cos(\gamma)}}{\lambda_u} \tag{25}$$

The angle of attack is assumed to respond much more quickly than the bank angle to control commands. Hence, we will treat angle of attack as the control ($u = \alpha$) and bank angle as a slowly varying parameter. We will use this parameter to reduce excursions in the angle of attack.

The equation for the "control costate" is then:

$$\dot{\lambda}_\alpha = -\lambda^T \frac{\partial f^T}{\partial\alpha} = \frac{\lambda_V}{m}\frac{\partial D}{\partial\alpha} - \frac{\lambda_\gamma \cos(\phi^*)}{mV^*}\frac{\partial L}{\partial\alpha} \tag{26}$$

It is possible that $\cos(\phi)$ is far from $\cos(\phi^*)$, so we also include

$$\dot{\lambda}^+_\alpha = \frac{\lambda_V}{m}\frac{\partial D}{\partial\alpha} - \frac{\lambda_\gamma}{mV^*}\frac{\partial L}{\partial\alpha} \tag{27}$$

which corresponds to $\cos(\phi) = 1$, and

$$\dot{\lambda}^-_\alpha = \frac{\lambda_V}{m}\frac{\partial D}{\partial\alpha} + \frac{\lambda_\gamma}{mV^*}\frac{\partial L}{\partial\alpha} \tag{28}$$

which corresponds to $\cos(\phi) = -1$. These three derivatives are used to produce three different values for λ_α. The value for λ_u used in equation 25 is determined by interpolating between the three values based on the current value of ϕ.

The bank angle is modulated to attempt to drive the angle of attack back to its nominal value.

$$\delta\phi = \begin{cases} \frac{\delta\alpha}{\delta\alpha_{max}}(180 - \|\phi\|) & \alpha > 0 \\ \frac{\delta\alpha}{\delta\alpha_{max}}(0 - \|\phi\|) & \alpha < 0 \end{cases} \tag{29}$$

Thus the control equations are:

$$\alpha_C = \alpha^* + \delta\alpha \tag{30}$$

and

$$\phi_C = \phi^* + \delta\phi \tag{31}$$

where $\delta\phi$ is from equation 29 and $\delta\alpha$ is from equation 25;

Out-of-Plane control

The preceding discussion only establishes the magnitude of the bank angle. The sign of the bank angle is used to control the final inclination or wedge angle. (Inclination is the angle between an orbit and the equator, while wedge angle is the angle between two orbits. The difference being that to achieve a zero wedge angle, one must match both inclination and longitude of ascending node.) The sign of the bank angle is reversed whenever the inclination or wedge angle exceeds deadband limits. The deadbands are specified as a function of velocity, typically with a funnel shape that narrows down as the exit velocity is approached. A "latch" logic is included so that once a bank reversal is initiated, it must be completed before another reversal can be commanded. The current work does not impose tight limits on the inclination.

Design Trajectory

It is clear from equations 30 and 31 that the algorithm depends strongly on the design trajectory. For the lowest ΔV, an ideal trajectory would exit the atmosphere full lift down and just meet the desired apoapsis. This would make the periapsis as high as possible. However, any atmospheric dispersions or vehicle modeling errors would cause the vehicle to fail to meet the required orbit. For increased robustness to atmospheric disturbances, the design trajectory has an angle of attack near the midpoint of its range and bank angle near 90 degrees.

MISSION

The current guidance scheme is applicable to any aerocapture mission with the capability of angle of attack modulation. For demonstration purposes, it was applied to a proposed mission of aerocapture at Neptune. One of the primary goals of this mission is a flyby of Neptune's moon, Triton. To match orbits with Triton, the vehicle must have an apoapsis of about 430,000 km. This is a particularly difficult aerocapture mission, because the atmospheric exit velocity must be so close the to escape velocity.

The preceding guidance algorithm was coded in Fortran and incorporated into the Program to Optimize Simulated Trajectories II (POST II)[8]. The atmosphere model used is NeptuneGram Version 0.

The vehicle chosen is a flat-bottomed ellipsled with nominal L/D of 0.8 at an angle of attack of 40 degrees. The vehicle has an entry mass of 2450.0 kg and a ballistic coefficient of 257.85 kg/m^2.

The entry states have a nominal entry flight path of 12.5 degrees. For Monte Carlo analysis, the states were provided at 60 seconds prior to atmospheric entry. The mean velocity was 28.85 km/s with a standard deviation of 0.01 km/s. The flight path angle variability was 0.175 deg 1-sigma. The axial force coefficient of the vehicle varied by $\pm$ 30% and the normal force coefficient varied by $\pm$ 50%.

NUMERICAL RESULTS

Nominal Trajectory

A nominal altitude-velocity curve is shown in figure 1. At the edge of Neptune's sensible atmosphere (taken as 25764 km radius), the escape velocity is 23 km/s. Figure 1 shows how close the exit condition is to escape velocity. The control histories from a nominal trajectory are shown in figure 2. The angle of attack is assumed to respond instantly to commands, while the bank angle has a simulated controller in the loop that limits bank accelerations to 5 deg/s^2 and bank rates to 20 deg/s.

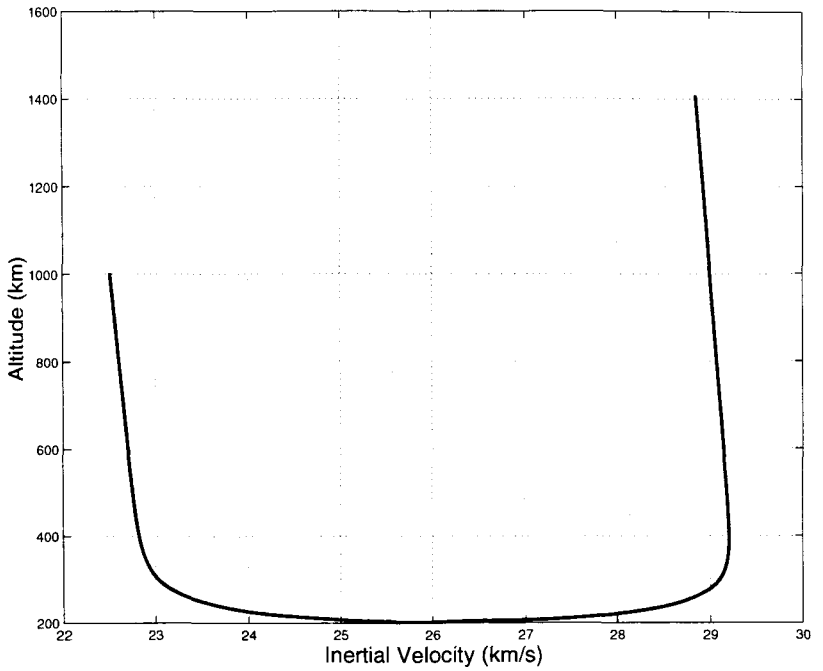

Figure 1: Nominal Altitude-Velocity curve.

Monte Carlo Analysis

Three Monte Carlo analyses were performed on three different versions of the α-modulated Terminal Point Controller. The three controllers differed in the range of angle-of-attack permitted. All three had a nominal angle-of-attack of 40 degrees, and the different versions were allowed excursions away from that of plus or minus 10, 5, and 3 degrees. As expected, as the allowable angle of attack range is reduced, performance is degraded, both in terms of accuracy of apoapsis as well as ΔV required.

Figure 3 shows the ΔV required to meet the target orbit versus inclination at atmosphere exit for 2000 Monte Carlo cases with and angle of attack range of $\pm$ 10 degrees. Figures 4 and 5 show the same results for angle of attack ranges of 5 and 3 degrees respectively. In Figure 3 the control of ΔV is very good most cases are less than 150 m/s with only a few above 200 m/s. When the angle of attack range is reduced to 5 degrees, Figure 4 shows that the ΔV values increase, some as high as 600 m/s. When the angle of attack range is further reduced to 3 degrees, Figure 5 shows that many of the ΔV values exceed 800 m/s.

Figure 6 shows the maximum sensed acceleration for each of the three monte carlo simulations. As can be seen the maximum acceleration increases as the angle of attack range increases. This increase is expected due to the higher lift force associated with higher angle of attack.

CONCLUSIONS

A guidance algorithm for aerocapture using angle of attack modulation as the primary control has been presented. Limitations have been imposed on the range of angle of attack allowed by the algorithm. Three different angle of attack ranges have been examined via Monte Carlo analysis. It has been shown that as the angle of attack range increases the performance of the guidance algorithm improves, but the sensed acceleration also increases with angle of attack range.

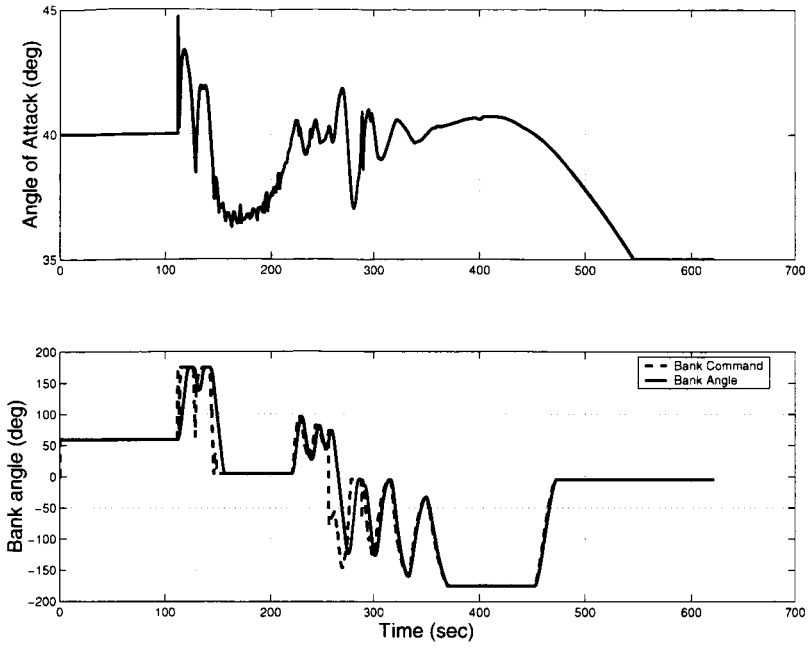

Figure 2: Nominal Control profiles.

References

[1] Striepe, et. al., "An Atmospheric Guidance Algorithm Testbed for the Mars Surveyor Program 2001 Orbiter and Lander," AIAA 98-4569, presented at AIAA Atmospheric Flight Mechanics Conference, August 10-12, 1998, Boston, Ma.

[2] Masciarelli, J. and Queen, E., "Guidance Algorithms for Aerocapture at Titan," AIAA 2003-4804, presented at 39^{th} AIAA/ASME/SAE/ASEE Joint Propulsion Conference and Exhibit, 2003.

[3] Rousseau, Stephane, and Fraysse, Hubert, "Study of the Mars Sample Return Orbiter Aerocapture Phase."

[4] *Apollo Guidance, Navigation and Control: Guidance System Operations Plan, Section 5 Guidance Equations*, Massachusetts Institute of Technology, Charles Stark Draper Laboratory, December, 1967.

[5] Bryson, Arthur E. and Ho, Yu-Chi, *Applied Optimal Control*, Hemisphere Publishing Corporation, Washington, D.C., 1975.

[6] Ro, T. and Queen, E., "Study of Martian Aerocapture Terminal Point Guidance," AIAA 98-4571, presented at AIAA Atmospheric Flight Mechanics Conference, August 10-12, 1998, Boston, Ma.

[7] Fraysse, H., Powell, R., Rousseau, S., Striepe, S., "CNES-NASA Studies of the Mars Sample Return Orbiter Aerocapture Phase," IAF-00-A.6.05, presented at 51^{st} International Astronautical Congress, 2-6 Oct, 2000, Rio de Janeiro, Brazil.

[8] Braur, G.L., Cornick, D.E., and Stevenson, R., "Capabilities and Applications of the Program to Optimize Simulated Trajectories (POST)," NASA CR-2770, February 1987.

[9] Carman, G., Ives, D, and Geller, D., "Apollo-Derived Mars Precision Lander Guidance," AIAA 98-4570, presented at AIAA Atmospheric Flight Mechanics Conference, August 10-12, 1988, Boston, Ma.

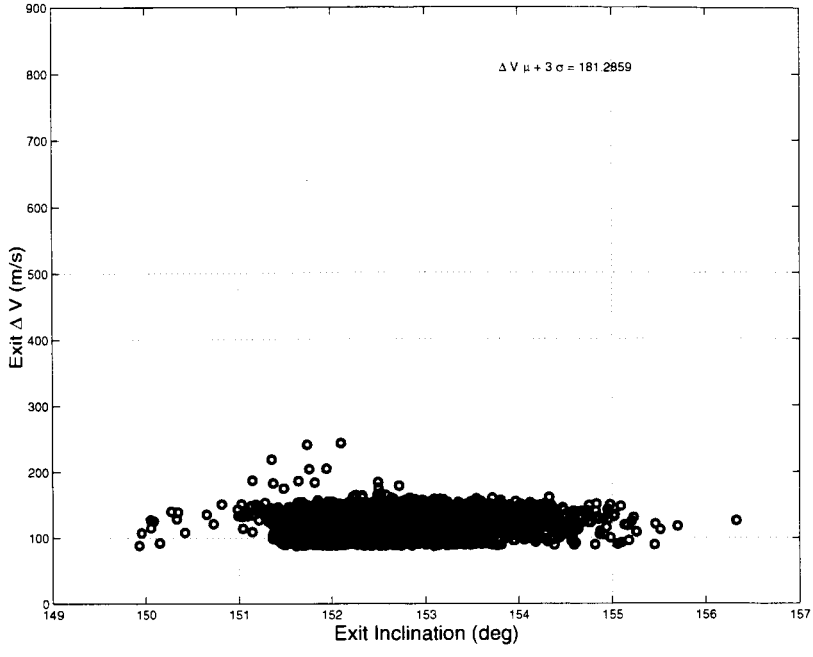

Figure 3: Ten degree Angle of Attack Range Monte Carlo.

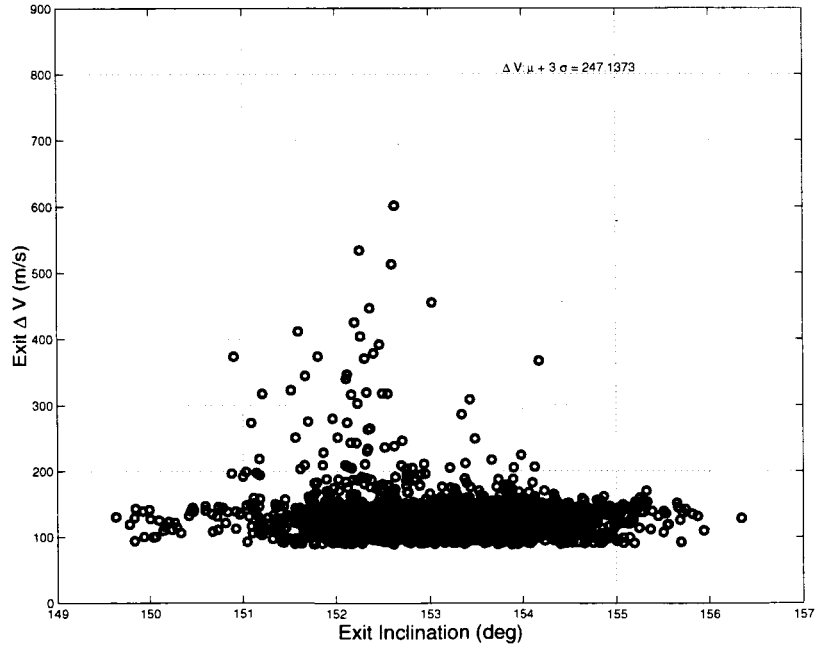

Figure 4: Five degree Angle of Attack Range Monte Carlo.

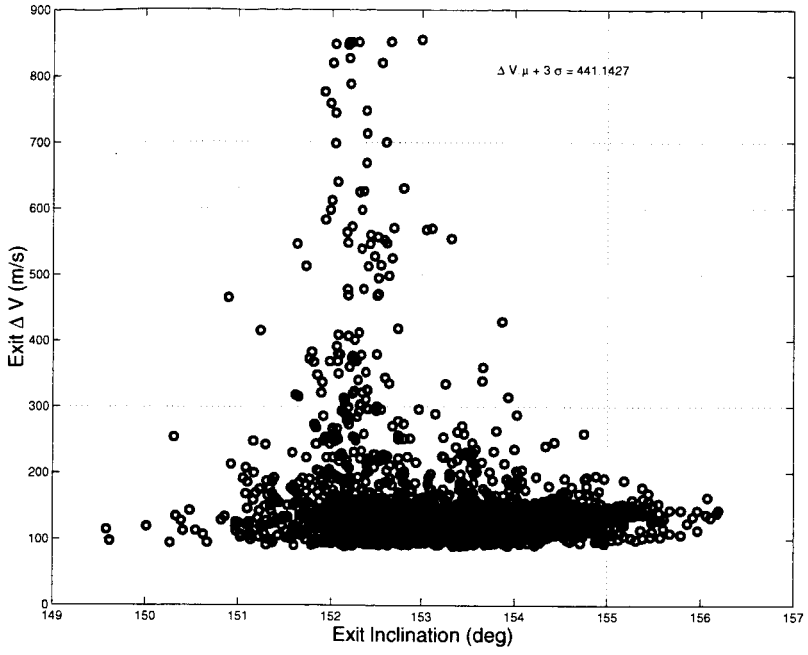

Figure 5: Three degree Angle of Attack Range Monte Carlo.

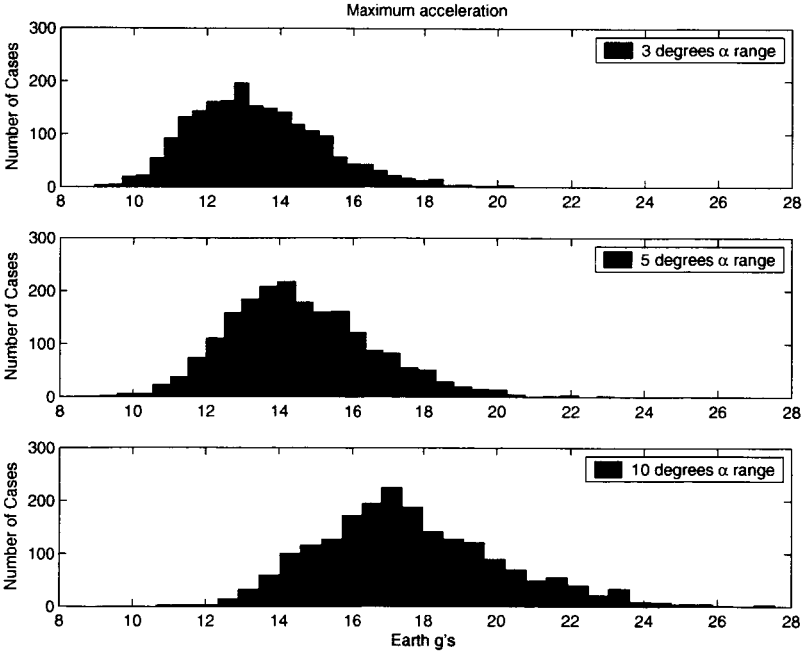

Figure 6: Maximum Sensed Acceleration.